Surface micromachining of polydimethylsiloxane for microfluidics applications

Staci Hill,[1,2] Weiyi Qian,[3] Weiqiang Chen,[1,3,a)] and Jianping Fu[1,4,5,6,a)]
[1]*Department of Mechanical Engineering, University of Michigan, Ann Arbor, Michigan 48109, USA*
[2]*Department of Chemistry and Biochemistry, Middlebury College, Middlebury, Vermont 05753, USA*
[3]*Department of Mechanical and Aerospace Engineering, New York University, Brooklyn, New York 11201, USA*
[4]*Department of Biomedical Engineering, University of Michigan, Ann Arbor, Michigan 48109, USA*
[5]*Department of Cell and Developmental Biology, University of Michigan Medical School, Ann Arbor, Michigan 48109, USA*
[6]*Michigan Center for Integrative Research in Critical Care, University of Michigan, Ann Arbor, Michigan 48109, USA*

(Received 21 July 2016; accepted 29 September 2016; published online 10 October 2016)

Polydimethylsiloxane (PDMS) elastomer has emerged as one of the most frequently applied materials in microfluidics. However, precise and large-scale surface micromachining of PDMS remains challenging, limiting applications of PDMS for microfluidic structures with high-resolution features. Herein, surface patterning of PDMS was achieved using a simple yet effective method combining direct photolithography followed by reactive-ion etching (RIE). This method incorporated a unique step of using oxygen plasma to activate PDMS surfaces to a hydrophilic state, thereby enabling improved adhesion of photoresist on top of PDMS surfaces for subsequent photolithography. RIE was applied to transfer patterns from photoresist to underlying PDMS thin films. Systematic experiments were conducted in the present work to characterize PDMS etch rate and etch selectivity of PDMS to photoresist as a function of various RIE parameters, including pressure, RF power, and gas flow rate and composition. We further compared two common RIE systems with and without bias power and employed inductively coupled plasma and capacitively coupled plasma sources, respectively, in terms of their PDMS etching performances. The RIE-based PDMS surface micromachining technique is compatible with conventional Si-based surface and bulk micromachining techniques, thus opening promising opportunities for generating hybrid microfluidic devices with novel functionalities. *Published by AIP Publishing*. [http://dx.doi.org/10.1063/1.4964717]

INTRODUCTION

Microfluidics has shown a significant promise in improving the way modern biological analyses are performed.[1–4] Integrated microfluidics provides the possibility of miniaturizing and integrating different biosample preparative and analytical techniques on a single chip to enable rapid, sensitive, and multiplexed high-throughput on-chip assays.[5–10] Polydimethylsiloxane (PDMS), a silicone-based organic polymer, has become the key material used in microfluidic applications. The intrinsic chemical structure of PDMS grants it favorable properties for biological applications. Siloxane chains of PDMS are responsible for its high thermal stability, while its organic backbone provides its mechanical elasticity and inert physiochemical properties.[11]

[a)]Authors to whom correspondence should be addressed. Electronic addresses: wchen@nyu.edu and jpfu@umich.edu

Additionally, PDMS is optically transparent, permeable to gases, and is an electric insulator, making it an ideal material for functional microfluidic systems.[12–14]

Currently, highly integrated microfluidic devices are most generated based on soft lithography of PDMS.[12] Soft lithography is a bulk micromachining method for PDMS, with the intrinsic difficulty in achieving a high fidelity patterning of surface structures with high resolution.[12] Using soft lithography, PDMS polymer is cured onto a resist or silicon mold to transfer the desired surface features from the mold to PDMS surfaces. Although convenient and efficient in creating microscale features (i.e., wells, channels, and chambers) with a thick, supportive PDMS base, it is difficult for soft lithography to produce high-resolution structures in PDMS thin films. Such surface microstructures, such as filtration membranes and free-standing beam structures, will be critical in advancing the overall complexity and functionalities of current microfluidic devices. For example, microfiltration devices have been used to isolate circulating tumor cells (CTCs).[15,16] In the area of immune cell analysis, a microfiltration membrane holds great significance for isolation of immune cell subsets. Yet, conventional microfiltration membranes have low effective porosity and are integrated in a difficult manner with PDMS devices which limit their biological applications. Free-standing beam structures are often required in microfluidic devices that served as force-based mechanical biosensors.[17] Integrating these free-standing surface microstructure units into a microfluidic device will greatly advance the application of microfluidics in bioengineering. However, technologies for surface micromachining (including both photolithographic patterning and dry/wet pattern transfer methods) to generate such functional structures on PDMS thin films are currently limited.

Previously, there have been several surface patterning methods being reported to achieve photolithographic patterning of regular structures on PDMS.[18–23] However, most of them suffer from constraints of limited resolution and/or alteration of physical and chemical properties of PDMS.[18–24] PDMS has been known incompatible with conventional lithography, due to a mismatch of its surface energy with photoresist that results in dewetting of photoresist on PDMS surfaces.[24] Although photolithography on PDMS surfaces can be achieved by introducing an intermediary adhesion layer on PDMS,[18–20] this intermediary adhesion layer is difficult to be removed after photolithography, causing additional constraints for device design and operation. Furthermore, chemical and physical properties of the adhesion layer-PDMS combination could divert from those properties of original PDMS.[18–20] Recently, it has been shown that PDMS can become photosensitive through chemical modification.[21–23] Thus, a direct photo-patterning of PDMS is applicable just like patterning photoresist in traditional lithography. Although the direct photo-patterning of photosensitive PDMS is attractive, there are potential drawbacks such as high cost and limited resolution. One additional major concern is that the biocompatibility of photosensitive PDMS has not been well characterized yet. Compared with the conventional PDMS that has long been used for biomedical applications, photosensitive PDMS presents a risk of introducing cytotoxicity. There is another method being developed using mechanical scrapping to achieve a thin PDMS membrane that can be transferred with functional structures from a silicon mold.[24] However, the minimum PDMS membrane thickness is restricted with its uniformity compromised.[24]

In addition to the difficulty in direct coating of photoresist on top of PDMS surfaces, transferring patterns from patterned photoresist to underlying PDMS is also challenging. Recent reports have shown both dry and wetting etching methods for patterning PDMS.[25–28] However, most of the attempts were still suboptimal, with limitations such as low etch rate, poor etching selectivity, and surface defects. For example, approaches using wet etching to create desired PDMS patterns still suffer from a limited resolution and poor selectivity. Undercutting and detachment of PDMS from underlying substrates were also observed during wet etching processes of PDMS.[28,29] Furthermore, a uniform etch rate was difficult to maintain in wet etching as the composition of etchent solution could vary during etching.[25] Dry etching can achieve anisotropic etch profile of different materials with good etching quality. However, most of the current dry etching systems, such as reactive-ion etching (RIE) systems, are designed for etching of semiconductor materials such as silicon and oxides. There is no standard and efficient dry etching technique available for etching polymers such as PDMS. Recent studies have

explored the possibility of dry etching of PDMS, yet shown very low etch rates.[18] In addition, because of intense ion collision on PDMS in dry etching, a substantial surface roughness on PDMS surfaces was observed, making it difficult to produce smooth surface features.[30] Additionally, etching selectivity was difficult to control for dry etching techniques.

Previously, we demonstrated a photolithographic surface patterning method to generate high-resolution features in PDMS thin films using conventional photolithography and RIE (Figs. 1 and 2).[31] This method incorporates a unique step of using oxygen plasma to activate PDMS surfaces to a hydrophilic state, thus enabling improved adhesion of photoresist on top of PDMS surfaces for subsequent photolithography (Fig. 1). RIE is then applied to transfer patterns from photoresist to underlying PDMS thin films. In the present study, we conducted systematic experiments to characterize PDMS etch rate and etch selectivity of PDMS to photoresist as a function of various RIE parameters, including RF power, total pressure, and gas flow rate and composition. We further compared two common RIE systems with and without bias RF power and employed inductively coupled plasma (ICP) and capacitively coupled plasma (CCP) sources, respectively, in terms of their PDMS etching performances. Our PDMS surface micromachining technique was compatible with the existing Si-based surface and bulk micromachining techniques, thus opening promising opportunities for generating hybrid microfluidic devices with novel functionalities.

MATERIALS AND METHOD

PDMS thin film preparation

A PDMS thin film was prepared by spin coating. Briefly, a Si wafer was first treated with oxygen plasma (Plasma Cleaner PDC-001, Harrick Plasma, Ithaca, NY) for 2 min before silanized with (tridecafluoro-1,1,2,2,-tetrahydrooctyl)-1-trichlorosilane vapor (United Chemical Technologies, Bristol, PA) for 1 h in vacuum to facilitate subsequent release of patterned PDMS layers. PDMS prepolymer (Sylgard-184, Dow Corning, Midland, MI) was prepared by thoroughly mixing PDMS curing agent with PDMS base monomer (*wt*:*wt* = 1:10). PDMS prepolymer was then spin-coated on the silanized Si wafer before cured at 100 °C for >4 h to generate PDMS thin layers with a thickness ranging from hundreds of microns down to ~2 μm. By adjusting the spin coating speed or the viscosity of PDMS (through diluting PDMS prepolymer with hexane), ultra-thin PDMS membranes with a submicron thickness could be fabricated.[32]

Surface activation and photolithographic surface patterning of PDMS

After preparation of thin PDMS layers on a Si wafer, PDMS surfaces were activated through a gentle oxygen plasma treatment under 20 W and 300 mTorr for 5 min to temporarily

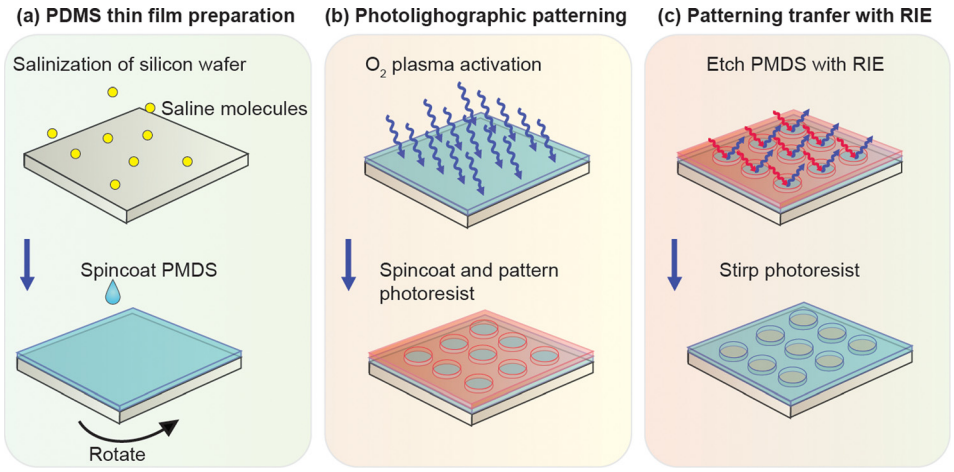

FIG. 1. Schematic showing photolithographic surface micromachining of PDMS.

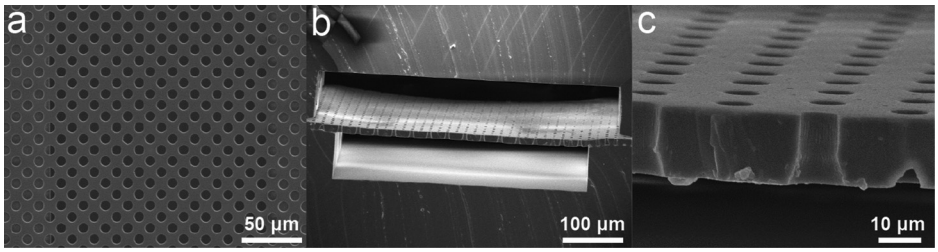

FIG. 2. Representative SEM images showing microfiltration membranes fabricated using the PDMS surface micromachining technique. (a) and (b) Top (a) and cross-sectional (b) views of PDMS microfiltration membranes sandwiched between two microfluidic channels. (c) High-magnification cross-sectional view of the PDMS microfiltration membrane. The membrane, with a thickness of 10 μm, contained an array of hexagonally spaced through holes with a hole diameter of 6 μm.

modify the original hydrophobic PDMS surface to a hydrophilic state. Photoresist (AZ 9260, AZ Electronic Materials, Branchburg, NJ) was then directly spin-coated on PDMS, soft-baked at 90 °C for 10 min, and patterned using conventional contact photolithography.

Pattern transfer by RIE

Photolithographically patterned Si wafers were processed using RIE to transfer patterns from photoresist to underlying PDMS layers. For RIE, either an ICP-based system (LAM 9400, Lam Research, Fremont, CA) or a CCP-based system (PlasmaTherm 790, Unaxis, Schwyz, Switzerland) was used. During RIE, reactive gas species would etch exposed PDMS regions anisotropically. Oxygen (O_2), sulfur hexafluoride (SF_6), tetrafluoromethane (CF_4), and octafluorocyclobutane (C_4F_8) were the gases used in the two RIE systems. Si wafers coated with PDMS layers were etched by RIE for 10–30 min. In the present work, RF power and bias power and gas composition and pressure were investigated to examine their independent effects on RIE etching of PDMS.

Characterization of PDMS film thickness, etch rate, and selectivity

Thicknesses of PDMS layers and photoresist were measured before and after RIE etching using a surface profilometer (Dektak 6M surface profiler, Veeco Instrument, Plainview, NY). Etch rate of PDMS by RIE was calculated as the PDMS layer thickness change divided by RIE etching time. Etch selectivity of PDMS was calculated as the ratio of etch rates of PDMS to photoresist during RIE etching.

Scanning electron microscopy (SEM) and atomic force microscopy (AFM)

SEM images were taken to inspect geometrical features of patterned PDMS layers. Briefly, samples were mounted on stubs, sputtered with gold palladium, observed and photographed under a Hitachi SU8000 Ultra-High Resolution SEM machine (Hitachi High Technologies America, Inc., Pleasanton, CA). Surface topology of PDMS layers was further characterized by AFM (Digital Instruments, Tonawanda, NY).

RESULTS AND DISCUSSION

Surface activation of PDMS for photolithographic patterning

A major challenge preventing direct photolithography of PDMS is the poor adhesion of photoresist on PDMS.[20,25] Nonpolar methyl backbone groups in PDMS make the PDMS surface extremely hydrophobic, prohibiting uniform coating of photoresist on PDMS surfaces, a critical step for conventional photolithography. Our method applying an oxygen plasma treatment on PDMS surfaces effectively addressed this technical issue by creating a temporary hydrophilic PDMS surface (Fig. 1). During oxygen plasma treatments, methyl groups on PDMS surfaces were destroyed while super-hydrophilic silanol groups were retained.[20,33] Although the effect of

oxygen plasma on hydrophobicity/hydrophilicity of PDMS surfaces was transient and reversible, spin-coating photoresist on PDMS immediately after their treatments with oxygen plasma would allow us to obtain a uniform photoresist coating on PDMS surfaces for subsequent photolithography (Fig. 1).

RIE with ICP and CCP systems

Etching of PDMS using RIE is resulted from both chemical and physical processes.[34] Etchant gases such as CF_4 and SF_6 are mainly used in RIE, given the reactive fluorine (F) molecules used for etching silicon and silicon dioxide. These molecules enter the RIE plasma chamber and are dissociated by a plasma to form fluorine radicals, which then diffuse into the PDMS surface, break the Si–O bond in PDMS, and produce volatile compounds (mainly SiF_4), thus etching PDMS.[28]

Etching of PDMS using RIE is influenced by DC bias voltage formed in the sheath of the plasma chamber.[35] Positive ions arriving over the sheath are accelerated by DC bias and bombard exposed PDMS surfaces, leading to increased vertical etch rate and promoting an anisotropic etching of PDMS. Ion bombardment also helps break the chemical bond of PDMS to form more active sites for fluorine to fill and react. Thus, increasing DC bias voltage leads to higher ion flux and results in a higher etch rate and high-aspect ratio etching. These contributions for PDMS etching by RIE, either from reactive radicals or the assist of ion bombardment, have been shown to have dependence on radio frequency (RF) power, process pressure, and etchant gases, which can influence the density of reactive radicals and the energy of bombarded ions.[36] Specifically, increasing RF power will increase the density of a plasma so as to increase the PDMS etch rate.[36] Adding a small fraction of O_2 (or N_2) into the feed gas will decrease the overall gas electronegativity and also may help to form volatile chemical compounds with polymers produced on PDMS surfaces, thus facilitating fluorine-assisted PDMS etching process.[37]

Different plasma reactors will also lead to diverse PDMS etching performances. The commonly used CCP reactor creates an electromagnetic field between two parallel electrodes to generate plasma for etching (Fig. 3(a)). The sheath DC bias voltage around the lower electrode helps in improving the anisotropy of ion flux into the substrate to be etched. To obtain a high DC bias for high aspect ratio etching, a low gas pressure is preferred for the CCP system. However, it is difficult to generate dense and uniform plasma at low pressure in the CCP reactor.[37] Together, these limitations of the CCP system prevent achieving high etching rate and high aspect etching ratio concurrently.

In ICP reactor, however, the electromagnetic field is generated by a RF current flowing through a coil, and such design enables a separate control of bias power using an alternative RF bias power source (Fig. 3(a)). The RF bias power in the ICP system can be used to independently control the energy of ion bombardment. Thus, in the ICP system, a dense plasma can be created at low pressure by controlling RF power, while the high energy ion bombardment can be obtained independently through RF bias power, making the ICP system suitable for creating high etching rate and highly anisotropic etching simultaneously. Thus, the ICP system might provide a relative better etching performance for PDMS micromachining in terms of efficiency and selectivity.

Effect of RF power on PDMS etching

We observed that the PDMS etch rate increased with increasing RF power in both ICP and CCP systems (Tables I and II and Fig. 3(b)), consistent with the fact that increasing RF power in both reactors had resulted in an increase of reactive radicals to accelerate PDMS etching. This is because that by increasing RF power, the density of a plasma in the chamber will increase. These dense fluorine radicals, which then diffuse into the PDMS surface, break the Si–O bond in PDMS. The more fluorine radicals reach the PDMS surface, the faster will the etch rate be. However, PDMS etch rate was distinct for each system (Fig. 3(b)), with the PDMS etch rate in ICP reactor much higher than that of the CCP reactor, which probably resulted from RF bias power available in the ICP reactor. The RF bias power in the ICP system drives the dense plasma to obtain high energy ion bombardment for creating high etching rate

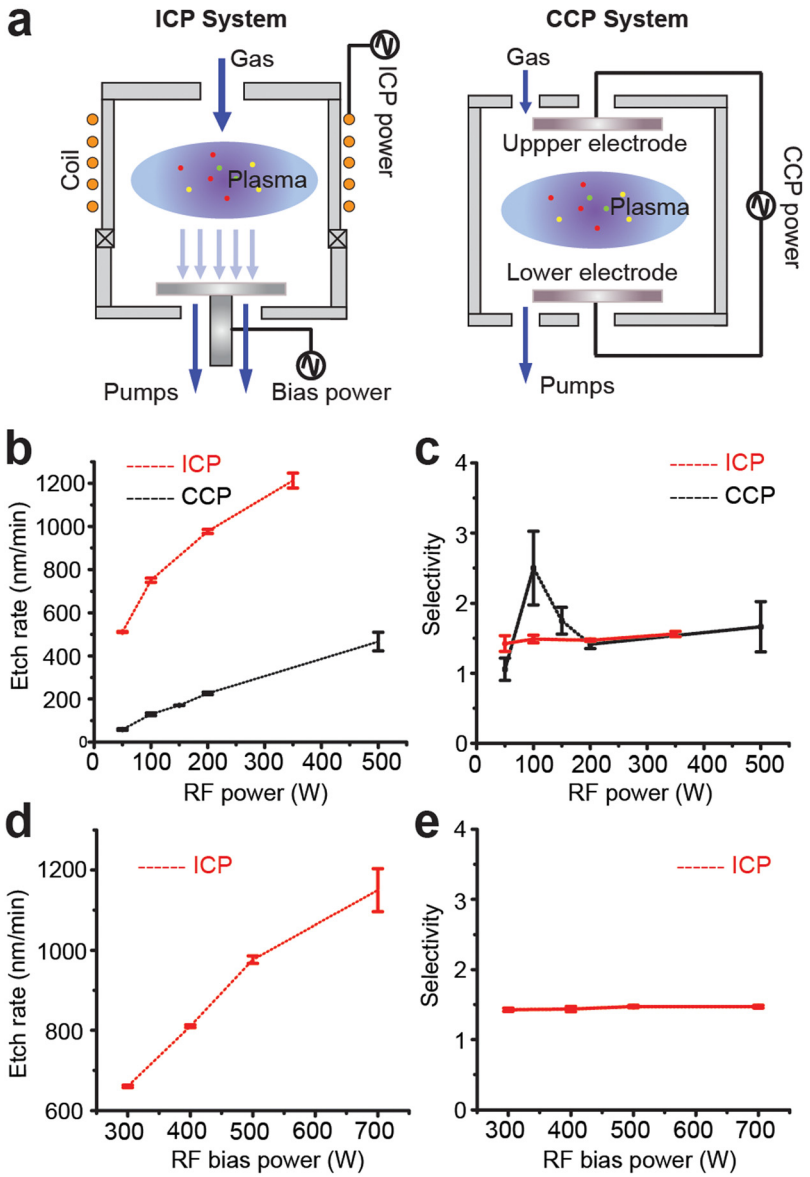

FIG. 3. PDMS etch rate and selectivity as a function of RF power in ICP and CCP systems. (a) Illustrations of ICP (left) and CCP (right) systems. (b) and (c) PDMS etch rate (b) and selectivity (c) as a function of RF power in ICP and CCP systems, as indicated. ICP system: RF bias power, 200 W; total pressure, 10 mTorr; etchant gases, 83.3% SF_6 and 16.7% O_2 with the total flow rate of 96 sccm. CCP system: RF bias power, 200 W; total pressure, 30 mTorr; etchant gases, 100% SF_6 with the total flow rate of 60 sccm. (d) and (e) PDMS etch rate (d) and selectivity (e) as a function of RF bias power in the ICP system. RF power, 500 W; total pressure, 10 mTorr; etchant gases, 83.3% SF_6 and 16.7% O_2 with the total flow rate of 96 sccm.

and highly anisotropic etching simultaneously. Consistently, increasing RF bias power in the ICP reactor also led to higher PDMS etch rates (Fig. 3(d)) with vertical PDMS etch profile (Fig. 2).

Even though for both ICP and CCP systems, the etch selectivity between PDMS and photoresist was maintained >1 under the power range applied (RF power: 0–500 W; RF bias power: 300–700 W), etch selectivity in the ICP system appeared constant (∼1.5) and showed little dependence on RF power or RF bias power (Figs. 3(c) and 3(e)). In contrast, increasing RF power in the CCP system first led to a rapid increase of etch selectivity to a maximum of 2.5 (with the RF power of 100 W), before the etch selectivity decreased with further increasing in RF power (Fig. 3(c)).

TABLE I. PDMS etch rate and selectivity as a function of RF power and RF bias power in the ICP system.

Sample	RF power (W)	RF bias power (W)	PDMS etch rate (μm/h)	Selectivity (PDMS/PR etch rate)
1	100	200	…	…
2	300	200	39.6	1.4
3	400	200	42.6	1.3
4	500	200	58.6	1.5
5	700	200	69.0	1.5
6	500	50	30.7	1.4
7	500	100	45.0	1.5
8	500	200	58.6	1.5
9	500	350	72.8	1.6

Effect of gas composition on PDMS etching

Etchant gases used in RIE etching of PDMS were also investigated in this work. Table III summarizes PDMS etching in the ICP and CCP systems using SF_6 and O_2. Here, etch power, total pressure, and total gas flow rate were maintained the same (specific values are listed in Fig. 4). Increasing proportions of SF_6 in the mixture of SF_6 and O_2 led to accelerated PDMS etching, which reached its maximum value of 70.7 μm h^{-1} (Fig. 4(c)) and 11.3 μm h^{-1} (Fig. 4(a)) in the ICP and CCP systems, respectively, with SF_6 ratio of 94% (ICP; Fig. 4(c)) and 100% (CCP; Fig. 4(a)). With the respective gas compositions for maximal PDMS etch rates, etch selectivity for each system also increased to its maximum value (ICP: 1.8 and CCP: 3.0; Figs. 4(b) and 4(d)).

Alternative fluorine based etchant gases C_4F_8 and CF_4 were also investigated for the ICP and CCP systems, respectively (Fig. 5). Compared with PDMS etching using SF_6, PDMS etch rates using C_4F_8 or CF_4 were relatively small (Figs. 5(a) and 5(c)). Specifically, biphasic dependence of PDMS etch rate on C_4F_8 (in ICP system) or CF_4 (in CCP system) compositions was observed. Too much C_4F_8 (in ICP system) or CF_4 (in CCP system), or an absence of O_2, led to negligible PDMS etch rates (Figs. 5(a) and 5(c)). However, if too little C_4F_8 or CF_4 in the CCP or ICP systems, respectively, PDMS etch rate started to decrease as well.

The presence of a small fraction of O_2 appeared to enhance PDMS etching in both CCP and ICP systems, with the mechanism not yet fully understood. It has been suggested that adding O_2 as RIE etchant gas helps reducing accumulation of polymers on substrates.[38] When only reactive gases are injected into RIE chambers, etching is hindered because the production rate of polymers on PDMS surface is greater than its etch rate that resulted from its reaction with fluorine. However, when O_2 is added, O and/or O_2 can react with polymers, preventing excess polymer accumulation on PDMS surface.

For RIE etching of PDMS using C_4F_8 or CF_4 as etchant gases, etch selectivity for PDMS was not as desirable as using SF_6 as the etchant gas (Figs. 5(b) and 5(d)). Therefore, SF_6/O_2 should be considered more desirable RIE etchant gases for PDMS surface micromachining.

Effect of total pressure on PDMS etching

The total pressure in the RIE process chamber also influences PDMS etch rate and selectivity (Table IV and Fig. 6). With constant RF powers and gas compositions and flow rates

TABLE II. PMDS etch rate and selectivity as a function of RF power in CCP system.

Sample	RF power (W)	PDMS etch rate (μm/h)	Selectivity (PDMS/PR etch rate)
1	50	3.5	1.1
2	100	7.7	2.5
3	150	10.3	1.8
4	200	13.6	1.4

TABLE III. PDMS etch rate and selectivity as a function of gas composition in ICP and CCP systems.

Sample	System	%SF_6	Etch Rate (μm/h)	Selectivity (PDMS/PR etch rate)
1	ICP	0	…	…
2	ICP	50	18.3	0.4
3	ICP	75	44.5	1.1
4	ICP	83	58.6	1.2
5	ICP	94	70.7	1.8
6	ICP	100	48.8	1.3
7	CCP	0	…	…
8	CCP	50	6.4	0.4
9	CCP	75	7.9	1.5
10	CCP	83	10.3	1.8
11	CCP	100	11.3	3.0

(specific values are listed in Fig. 6), in the ICP system, PDMS etch rate decreased rapidly as the total pressure increased (Fig. 6(a)). The effect of total pressure on PDMS etch selectivity in the ICP system was less pronounced (Fig. 6(b)). A probable explanation for the effect of total pressure on PDMS etch rate was that at higher pressure, the time of reactive radicals staying on PDMS surface would increase, preventing timely renewal of reactive radicals, thus resulting in lower PDMS etch rate. Thus, the total pressure should be kept low in the ICP system to achieve high PDMS etch rate.

In the CCP system, PDMS etch rate reached a maximum as the total pressure increased to 100 mTorr, before decreased upon further increase of the total pressure (Fig. 6(a)). A similar

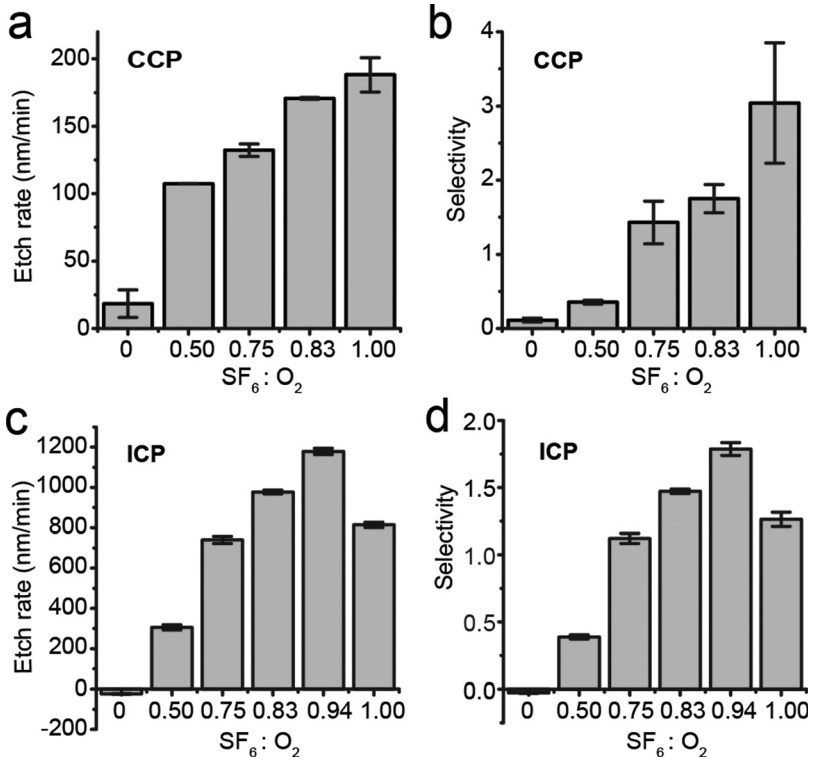

FIG. 4. PDMS etch rate (a) and (c) and selectivity (b) and (d) as a function of SF_6 / O_2 gas composition in CCP and ICP systems as indicated. CCP system: RF power, 150 W; total pressure, 30 mTorr; total gas flow rate, 60 sccm. ICP system: RF power, 500 W; RF bias power, 200 W; total pressure, 10 mTorr; total gas flow rate, 96 sccm.

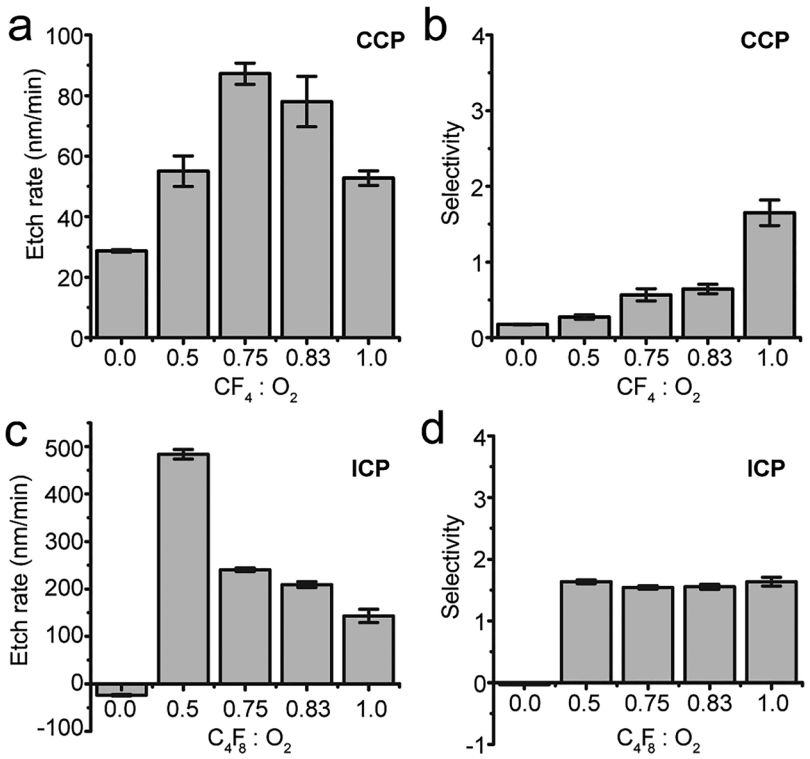

FIG. 5. PDMS etch rate (a) and (c) and selectivity (b) and (d) as a function of CF_4 (C_4F_8)/O_2 gas composition in CCP and ICP systems as indicated. CCP system: RF power, 150 W; total pressure, 30 mTorr; total gas flow rate, 60 sccm. ICP system: RF power, 500 W; RF bias power, 200 W; total pressure, 10 mTorr; total gas flow rate, 96 sccm.

biphasic response of PDMS etch selectivity was also observed as the total pressure increased from 25 mTorr to 250 mTorr. Such biphasic responses of PDMS etch rate and selectivity to the total pressure in the CCP system might be related to the density of plasma.[37] However, a detailed understanding of the underlying mechanism remains elusive and is out of scope of the present study.

Other observations of RIE etching of PDMS

During RIE etching of PDMS, heat would accumulate and if not dispensed on time, photoresist would char. It should also be noted that in photolithography, sudden temperature changes after soft bake of photoresist should be avoided, as cracks could easily develop in photoresist

TABLE IV. PDMS etch rate and selectivity as a function of total pressure in ICP and CCP systems.

Sample	System	Total pressure (mTorr)	Etch rate (μm/h)	Selectivity (PDMS/PR etch rate)
1	ICP	10	58.6	1.2
2	ICP	50	35.1	1.5
3	ICP	100	26.4	1.6
4	ICP	150	13.7	1.4
5	CCP	30	10.3	1.8
6	CCP	50	11.1	2.2
7	CCP	100	13.3	2.6
8	CCP	150	12.1	2.8
9	CCP	200	8.8	2.2
10	CCP	250	1.1	0.2

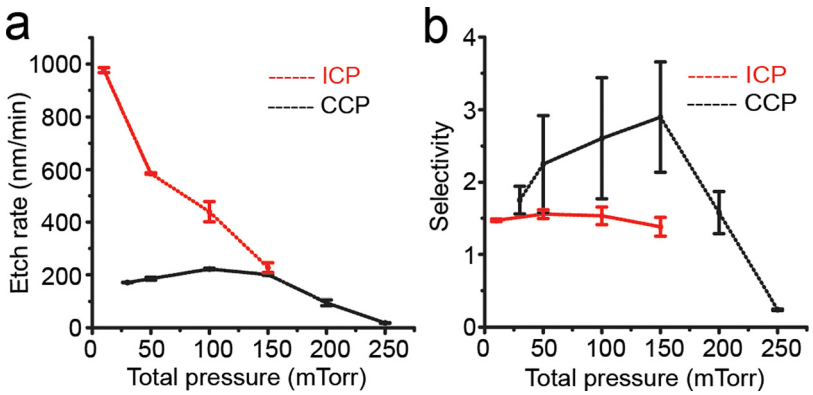

FIG. 6. PDMS etch rate (a) and selectivity (b) as a function of the total chamber pressure in ICP and CCP systems as indicated. ICP system: RF power, 500 W; RF bias power, 200 W; etchant gases, 83.3% SF_6 and 16.7% O_2 with a total flow rate of 96 sccm. CCP system: RF power, 150 W; etchant gases, 83.3% SF_6 and 16.7% O_2 with a total flow rate of 60 sccm.

due to a mismatch of the coefficient of thermal expansion (CTE) between PDMS and photoresist.

It is worth noting that RF power and RIE etching time could both affect the anisotropic etching profile of PDMS, as excessive RF power or RIE etching time had often led to a slanted sidewall of etched PDMS structures. When using CF_4 and O_2 gases to etch PDMS, a large surface roughness ($\sim\mu$m) on etched PDMS surface was observed; such PDMS surface roughness was not observed when using SF_6 and O_2 gases. Such PDMS surface roughness generation when using CF_4 and O_2 gases has been explained elsewhere that the difference in etch rates of organic parts and inorganic backbone of PDMS chains results in the formation of columnar-like structures on etched PDMS surface.[39]

Although both the ICP and CCP systems achieved satisfactory patterning resolutions, the ICP system equipped with a cryogenetic chuck generated a clean and vertical sidewall in etched PDMS structures (Figs. 7(a) and 7(b)). In comparison, features generated by the CCP system in PDMS thin films were relatively rough (Figs. 7(c) and 7(d)).

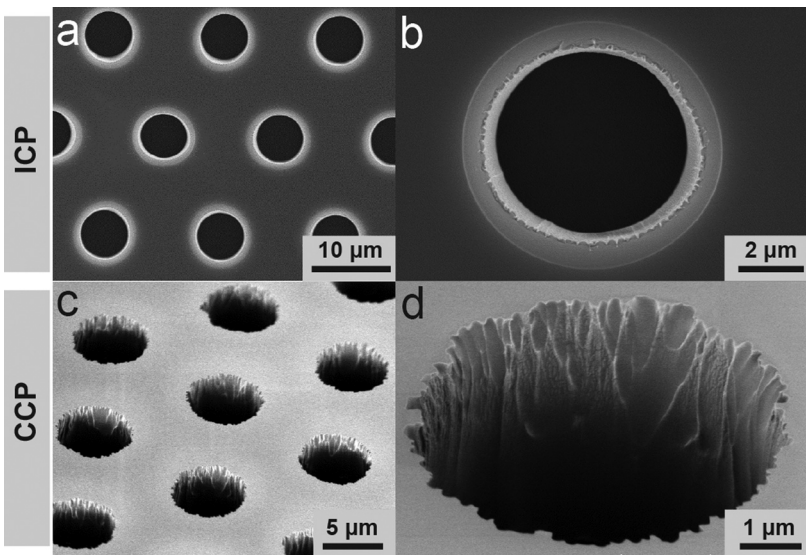

FIG. 7. Representative SEM images showing PDMS microfiltration membranes fabricated using ICP (a) and (b) and CCP (c) and (d) systems as indicated. The PDMS microfiltration membrane, with a thickness of 10 μm, contained an array of hexagonally spaced through holes with a hole diameter of 6 μm. ICP system: RF power, 500 W; RF bias power, 200 W; total pressure, 10 mTorr; etchant gases, 83.3% SF_6 and 16.7% O_2 with a total flow rate of 96 sccm. CCP system: RF power, 100 W; total pressure, 30 mTorr; etchant gases, 83.3% SF_6 and 16.7% O_2 with a total flow rate of 60 sccm.

TABLE V. Summary of RIE parameters in ICP and CCP systems for optimal PDMS etching.

Plasma System	RF power (W)	Total pressure (mTorr)	Gas composition	Etch rate (nm/min)	Etch selectivity
CCP	100	30	100% SF_6	188	2.6
ICP	500	10	94% SF_6	1,180	1.8

CONCLUSION

In summary, we introduced a PDMS surface micromachining method using direct photolithography followed by RIE for applications in functional microfluidics. Independent effects of different RIE parameters including RF power, gas composition and flow rate, and chamber pressure on PDMS etching were explored in order to achieve a high PDMS etch rate, good etch selectivity between PDMS and photoresist, as well as satisfactory PDMS etch quality (anisotropic etching with smooth etched surfaces).

Optimal PDMS etching recipes were determined for both ICP and CCP systems regarding PDMS etch rate and selectivity and quality of etched PDMS structures (Table V). PDMS etch rates in both ICP and CCP systems were predominantly influenced by gas composition, RF power, and gas pressure. Overall, PDMS etch rate in the ICP system was a magnitude greater than that of the CCP system. This significant PDMS etch rate difference was largely due to the maximum RF power that each system could provide while maintaining a good quality of PDMS etching. Due to the absence of cryogenic chuck in the CCP system, the maximum RF power in the CCP system was limited. Furthermore, RF bias power in the ICP system played a beneficial role in providing accelerated and directional ion bombardment contributing to faster and highly anisotropic PDMS etching. Different etchant gases SF_6/O_2, C_4F_8/O_2, and CF_4/O_2 were investigated in the PDMS etching process. Compared with C_4F_8/O_2 and CF_4/O_2, SF_6-based etchant gases that appeared most effective for PDMS etching in both ICP and CCP systems in terms of PDMS etch rate and selectivity as well as satisfactory PDMS etch quality.

Our PDMS surface micromachining technique possesses great potential for generating hybrid microfluidic devices with novel functionalities.[40–45] For example, using the RIE-based PDMS surface micromachining technique, we have successfully achieved wafer-scale fabrication of different planar PDMS microstructures (thicknesses of 0.2–10 μm), including PDMS-based free-standing cantilever structures and large microfiltration membranes containing arrays of through-holes (hole diameter of 6 – 20 μm) with a high porosity (up to 30%).[46,47] The high-porosity microfiltration membranes have been integrated in microfluidic devices for high-throughput processing of raw blood specimens without clogging.[46,47] Such PDMS microfiltration membranes could potentially be applied for size-based separation of circulating tumour cells (CTCs) from whole blood samples.[48] Since geometries of etched PDMS structures are defined by photolithography, the size and pattern of such structures could be precisely controlled with high resolution. Additionally, the RIE-based PDMS surface micromachining technique is compatible with other traditional Si-based surface and bulk micromachining techniques. Thus, highly integrated microfabrication involving both PDMS and Si-based materials becomes possible, which will provide exciting opportunities for generating hybrid microfluidic devices with well-defined functional PDMS microstructures for advanced bioengineering applications.

ACKNOWLEDGMENTS

We acknowledge the financial support from the National Science Foundation (Grant Nos. ECCS 1231826, CBET 1263889, and CMMI 1536087), the National Institutes of Health (Grant No. R01 HL119542), and the Michigan Center for Integrative Research in Critical Care (Grant No. M-CIRCC). W. Chen and W. Qian were partially supported by the New York University Global Seed Grant and the American Heart Association Scientist Development Grant

(No. 16SDG31020038). The Lurie Nanofabrication Facility at the University of Michigan, a member of the National Nanotechnology Infrastructure Network (NNIN) funded by the National Science Foundation, is acknowledged for support in microfabrication.

[1]E. K. Sackmann, A. L. Fulton, and D. J. Beebe, Nature **507**(7491), 181–189 (2014).
[2]G. M. Whitesides, Nature **442**(7101), 368–373 (2006).
[3]P. S. Dittrich and A. Manz, Nat. Rev. Drug Discovery **5**(3), 210–218 (2006).
[4]C. Rivet, H. Lee, A. Hirsch, S. Hamilton, and H. Lu, Chem. Eng. Sci. **66**(7), 1490–1507 (2011).
[5]K. Pantel, R. H. Brakenhoff, and B. Brandt, Nat. Rev. Cancer **8**(5), 329–340 (2008).
[6]L. Ren, Y. Chen, P. Li, Z. Mao, P.-H. Huang, J. Rufo, F. Guo, L. Wang, J. P. McCoy, and S. J. Levine, Lab Chip **15**(19), 3870–3879 (2015).
[7]M. Yu, S. Stott, M. Toner, S. Maheswaran, and D. A. Haber, J. Cell Biol. **192**(3), 373–382 (2011).
[8]P. Li, Z. Mao, Z. Peng, L. Zhou, Y. Chen, P.-H. Huang, C. I. Truica, J. J. Drabick, W. S. El-Deiry, and M. Dao, Proc. Natl. Acad. Sci. **112**(16), 4970–4975 (2015).
[9]C. Alix-Panabières and K. Pantel, Nat. Rev. Cancer **14**(9), 623–631 (2014).
[10]P. Li, Z. S. Stratton, M. Dao, J. Ritz, and T. J. Huang, Lab Chip **13**(4), 602–609 (2013).
[11]J. R. Anderson, D. T. Chiu, H. Wu, O. Schueller, and G. M. Whitesides, Electrophoresis **21**(1), 27–40 (2000).
[12]Y. Xia and G. M. Whitesides, Annu. Rev. Mater. Sci. **28**(1), 153–184 (1998).
[13]J. Brugger, G. Beljakovic, M. Despont, H. Biebuyck, N. De Rooij, and P. Vettiger, Sens. Actuators, A **70**(1), 191–194 (1998).
[14]A. Mata, A. J. Fleischman, and S. Roy, Biomed. Microdevices **7**(4), 281–293 (2005).
[15]H. K. Lin, S. Zheng, A. J. Williams, M. Balic, S. Groshen, H. I. Scher, M. Fleisher, W. Stadler, R. H. Datar, and Y.-C. Tai, Clin. Cancer Res. **16**(20), 5011–5018 (2010).
[16]S. Zheng, H. K. Lin, B. Lu, A. Williams, R. Datar, R. J. Cote, and Y.-C. Tai, Biomed. Microdevices **13**(1), 203–213 (2011).
[17]J. Arlett, E. Myers, and M. Roukes, Nat. Nanotechnol. **6**(4), 203–215 (2011).
[18]K. W. Meacham, R. J. Giuly, L. Guo, S. Hochman, and S. P. DeWeerth, Biomed. Microdevices **10**(2), 259–269 (2008).
[19]N. Bowden, S. Brittain, A. G. Evans, J. W. Hutchinson, and G. M. Whitesides, Nature **393**(6681), 146–149 (1998).
[20]R. M. Diebold and D. R. Clarke, Lab Chip **11**(9), 1694–1697 (2011).
[21]S. P. Desai, B. M. Taff, and J. Voldman, Langmuir **24**(2), 575–581 (2008).
[22]A. A. S. Bhagat, P. Jothimuthu, and I. Papautsky, Lab Chip **7**(9), 1192–1197 (2007).
[23]J. Lötters, W. Olthuis, P. Veltink, and P. Bergveld, J. Micromech. Microeng. **7**(3), 145 (1997).
[24]K. S. Ryu, X. Wang, K. Shaikh, and C. Liu, J. Microelectromech. Syst. **13**(4), 568–575 (2004).
[25]S. J. Hwang, D. J. Oh, P. G. Jung, S. M. Lee, J. S. Go, J.-H. Kim, K.-Y. Hwang, and J. S. Ko, J. Micromech. Microeng. **19**(9), 095010 (2009).
[26]G. Bjoørnsen and J. Roots, J. Vac. Sci. Technol., B: Microelectron. Nanometer Struct. **29**(1), 011001 (2011).
[27]B. Balakrishnan, S. Patil, and E. Smela, J. Micromech. Microeng. **19**(4), 047002 (2009).
[28]J. Garra, T. Long, J. Currie, T. Schneider, R. White, and M. Paranjape, J. Vac. Sci. Technol., A **20**(3), 975–982 (2002).
[29]N. Lucas, S. Demming, A. Jordan, P. Sichler, and S. Büttgenbach, J. Micromech. Microeng. **18**(7), 075037 (2008).
[30]D. Szmigiel, K. Domański, P. Prokaryn, P. Grabiec, and J. W. Sobczak, Appl. Surf. Sci. **253**(3), 1506–1511 (2006).
[31]W. Chen, R. H. Lam, and J. Fu, Lab Chip **12**(2), 391–395 (2012).
[32]A. L. Thangawng, R. S. Ruoff, M. A. Swartz, and M. R. Glucksberg, Biomed. Microdevices **9**(4), 587–595 (2007).
[33]A. Plecis and Y. Chen, Microelectron. Eng. **85**(5–6), 1334–1336 (2008).
[34]G. Bjørnsen, L. Henriksen, J. H. Ulvensøen, and J. Roots, Microelectron. Eng. **87**(1), 67–71 (2010).
[35]E. Mateev and I. Zhelyazkov, J. Phys. D: Appl. Phys. **32**(23), 3019 (1999).
[36]H. Jansen, H. Gardeniers, M. deBoer, M. Elwenspoek, and J. Fluitman, J. Micromech. Microeng. **6**(1), 14–28 (1996).
[37]P. Verdonck, Oficina de Microfabrição: Projeto e Construção de CI's MOS (2006).
[38]Y. N. Grigoryev and A. Gorobchuk, Russ. Microelectron. **36**(5), 321–332 (2007).
[39]A. Tserepi, M. Vlachopoulou, and E. Gogolides, Nanotechnology **17**(15), 3977 (2006).
[40]N.-T. Huang, W. Chen, B.-R. Oh, T. T. Cornell, T. P. Shanley, J. Fu, and K. Kurabayashi, Lab Chip **12**(20), 4093–4101 (2012).
[41]W. Li, Z. Xu, J. Huang, X. Lin, R. Luo, C.-H. Chen, and P. Shi, Sci. Rep. **4**, 4784 (2014).
[42]M. Bračič, T. Mohan, R. Kargl, T. Griesser, S. Hribernik, S. Köstler, K. Stana-Kleinschek, and L. Fras-Zemljič, RSC Adv. **4**(23), 11955–11961 (2014).
[43]T. S. Santisteban, R. Zengerle, and M. Meier, RSC Adv. **4**(89), 48012–48016 (2014).
[44]M. E. Moustafa, V. S. Gadepalli, A. A. Elmak, W. Lee, R. R. Rao, and V. K. Yadavalli, J. Biol. Eng. **8**(1), 24 (2014).
[45]M. E. Warkiani, A. A. S. Bhagat, B. L. Khoo, J. Han, C. T. Lim, H. Q. Gong, and A. G. Fane, ACS Nano **7**(3), 1882–1904 (2013).
[46]W. Chen, N. T. Huang, B. Oh, R. H. Lam, R. Fan, T. T. Cornell, T. P. Shanley, K. Kurabayashi, and J. Fu, Adv. Healthcare Mater. **2**(7), 965–975 (2013).
[47]X. Li, W. Chen, G. Liu, W. Lu, and J. Fu, Lab Chip **14**(14), 2565–2575 (2014).
[48]W. Qian, Y. Zhang, and W. Chen, Small **11**(32), 3850–3872 (2015).